Low activity microstates during sleep

Hiroyuki Miyawaki (1), Yazan N. Billeh (2), Kamran Diba (1)

(1) Dept of Psychology, Box 413, University of Wisconsin—Milwaukee, Milwaukee, WI 53201

(2) Computation and Neural Systems Program, California Institute of Technology, Pasadena, CA 91125

Running head: LOW activity sleep

*Correspondence to: diba@uwm.edu

Acknowledgements: We are grateful to Adrien Peyrache, Kenji Mizuseki, and crcns.org for making their data readily available, and Christof Koch, Markus Schmidt, Brendon Watson for valuable comments. H.M. and K.D. designed research and wrote the manuscript. H.M. performed research. Y.N.B. performed analyses identifying LOW-active cells.

Abstract (240 words)

To better understand sleep requires evaluating the distinct activity patterns of the brain during sleep. We performed extracellular recordings of large populations of hippocampal region CA1 neurons in freely moving rats across sleep and waking states. Throughout non-REM (non-rapid eye movement) sleep, we observed periods of diminished oscillatory and population spiking activity lasting on the order of seconds, distinct from characterized DOWN states, which we refer to as "LOW" activity sleep states. LOW states lasted longer than characterized DOWN states and were distinguished by a subset of "LOW-active" cells. LOW activity sleep was preceded and followed by increased sharp-wave ripple (SWR) activity. We also observed decreased slow-wave activity (SWA) and sleep spindles in the hippocampus local-field potential (LFP) and neocortical electroencephalogram (EEG) upon LOW onset, but only a partial rebound immediately after LOW. LOW states demonstrated LFP, EEG, and electromyogram (EMG) patterns consistent with sleep, but otherwise resembled previously described small-amplitude irregular activity (SIA) during quiet waking. Their likelihood increased over the course of sleep, particularly following REM sleep. To confirm that LOW is a brain-wide phenomenon, we analyzed data from the entorhinal cortex of rats, medial prefrontal cortex, and anterior thalamus of mice, obtained from crcns.org and confirmed that LOW states corresponded to markedly diminished activity simultaneously in all of these regions. We propose that LOW states are an important microstate within non-REM sleep that provide respite from high-activity sleep, and prepare the brain for a transition to waking.

Significance Statement (92 words)

In large-population neural recordings from sleeping rats, we observed long-lasting LOW activity epochs during which neuronal spiking and oscillatory activities were suppressed. By incorporating data from multiple brain regions, we observed that LOW states are a far-reaching phenomenon and not restricted to the hippocampus. The likelihood of occurrence of LOW activity states varied inversely with sleep pressure, increasing with time asleep, particularly after REM, and decreasing following time awake. We propose that these LOW activity states allow neurons to rest and repair and provide potential windows for transitions between sleep and awake.

Introduction (468 words)

The brain passes through multiple distinct stages during sleep. Each stage produces distinct activity patterns, presumably playing important roles in the function of the brain. Non-REM (non-rapid eye movement) sleep, in particular, has been associated with sleep homeostasis (1), synaptic plasticity (2), memory consolidation (3), and a host of other sleep functions (4). The signature activity pattern of non-REM sleep is the slow oscillation, an approximately 1 Hz alternation in cortical populations between UP states with robust spiking activity and DOWN states where most neurons are silent (5). During UP states, activity patterns can further display various faster oscillations, including sleep spindles (10-16 Hz) and hippocampal sharp-wave ripples (SWRs; 130 – 230 Hz) (6). On the other hand, DOWN states are characterized by the lack of any spiking activity, lasting on the order of ~100 ms (7).

A number of sleep functions have been attributed to the slower, longer lasting microstates of the brain. For example, the transition from the DOWN to the UP state during the slow oscillation can synchronize activity across the brain and provide a window for information transfer between the hippocampus and neocortex (8, 9). Meanwhile, the transition to the DOWN state could induce synaptic long-term depression (10) in cortical networks. The DOWN state also provides neurons with respite from intensive discharge and ionic flux. It has been suggested that this respite allows for more efficient cellular restoration and maintenance (11). Even longer lasting low and high activity phases have been reported during “infra-slow” oscillations under anesthesia and waking (12-16). The high activity phases of these oscillations have been linked to

"default mode" networks that subserve cognition (12, 14, 17), while the low activity phases reflect decreased blood flow and metabolic cost (18).

Recently, we performed long duration recordings from the hippocampus and neocortex of freely moving and sleeping rats and report the prevalence of low firing periods that lasted several seconds, far beyond the durations attributed to DOWN states. Following Pickenhain and Klingberg (19) and Bergmann et. al. (20), and because of their effects on neuronal firing, we call these "LOW" activity sleep states, but they have also been called "sleep small-amplitude irregular activity" (S-SIA; 21). We reserve the term SIA, as it was originally used, to describe quiet waking patterns (22). We evaluate the occurrence of LOW activity sleep across the circadian cycle, and describe its effects on other oscillatory activities within non-REM sleep, including slow-wave activity (SWA), sleep spindles, and sharp-wave ripples, and on firing rates of neurons in the hippocampus and other brain regions. We contrast these with SIA states during quiet waking, that are similar to LOW but display different electromyogram (EMG), local field potential (LFP) and electroencephalogram (EEG) patterns. We conjecture that LOW states provide neuronal rest within sleep and may prepare the brain for transitioning into quiet waking.

Results

Long lasting LOW activity states during non-REM sleep

We performed spike-detection and unit-isolation of CA1 neurons on multiple sessions from both light and dark cycles, in four animals, yielding 19-179 (M = 84.2) well-isolated pyramidal cells/session, 1–22, M = 7.3 putative interneurons/session, and 1-43, M = 11.2 multi-unit clusters. In population spike rasters recorded in different animals during non-REM, we observed striking and sporadic epochs of diminished activity that lasted for

several seconds (Figure 1A-C). These epochs, which we hereafter refer to as "LOW" states, appeared as "vertical" stripes in population spiking activity and were accompanied by strongly diminished power in the LFP. To detect these low activity/low amplitude epochs independently of firing rates, we calculated and set thresholds on the spectral power < 50 Hz in the LFP (Figure 1B, D; see Materials and Methods). Histograms of this low-passed LFP power showed two peaks in non-REM, reflecting LOW and non-LOW sleep (Figure 1B). In contrast, histograms of LFP power had only one peak in other behavioral states. As noted, neuronal firing rates during LOW sleep were strongly diminished (Figure 1A, C, E). To confirm this observation statistically, we calculated a modulation index (*MI*) for the firing rate of each cell within and outside of LOW states with non-REM (see Materials and Methods). The distribution of *MI* was heterogeneous (Figure 1E and H), with a small subset of cells showing significantly positive *MI* (see Materials and Methods). Overall, the mean *MI* was significantly < 0 for pyramidal cells (*MI* = -0.50 ± 0.01, $p = 1.5 \times 10^{-243}$, Wilcoxon signed- rank test), multi-units (*MI* = -0.65 ± 0.02, $p = 2.2 \times 10^{-35}$, Wilcoxon signed-rank test) and interneurons (*MI* = -0.19 ± 0.02, $p = 6.5 \times 10^{-12}$, Wilcoxon signed-rank test), indicating that while LOW states had a lesser effect on inhibitory cells, they were not a result of enhanced inhibition.

In these recordings, we observed right-skewed distributions for the durations of LOW states (median = 5.2 s, range: 1.0 s to 129.8s in 15,573 events), and their inter-event intervals (median = 10.5 s; Figure 1F). The 1-s windows we used for spectral calculations put a lower limit on the duration of detectable LOW states. Nevertheless, the mode of the histogram was at 3.5 s. The distributions of these variables were also right-skewed for DOWN states detected using standard methods (7, 23), but with shorter durations

(median = 0.081 s, range: 0.050-3.494 s), and inter-event intervals (median = 0.084 s). No secondary peaks were observed in the any of the histograms, indicating the absence of oscillatory repeated cycles. On average 45.8% of LOW (n = 19 sessions) overlapped with a DOWN state. However, DOWN states rarely lasted > 2s (14 out of 1.3 x 10^6 detected DOWNs). An alternate method of DOWN detection (24) tuned for the hippocampus yielded very similar results (median duration = 0.070s; range: 0.010 – 4.900 s; see also Ji and Wilson's (24) Supplementary Figure 12d), with only 51 DOWN states > 2s.

To further rule out the possibility that LOW states are long-lasting DOWN states, we relaxed the threshold of DOWN beyond standard criterion to yield low-firing DOWN' states (Figure 1G). The MUA firing rate threshold (24) was iteratively increased for each session until the median firing rates of LOW and DOWN' states were equal. In sum, 81.5% (n = 19 sessions) of LOW was in such DOWN' states but 63.3% of DOWN' occurred outside of detected LOW. Likewise, when we looked exclusively at long DOWN' states > 2s, 54.8% of LOW states were in long DOWN' while 38.7% of long DOWN' was outside of LOW. Thus, LOW and DOWN' states overlapped but were not identical. As expected, virtually all (Figure 1H, 98.9% of n = 1599) neurons were significantly suppressed during DOWN' states. However, a subset of neurons were active specifically during LOW states (5.9% of n = 1599, $p = 3.0 \times 10^{-269}$, chi-square test; see also Figure 2D). Previous work indicates that these hippocampal "LOW-active" cells have place fields within the animal's sleep environment (21, 25, 26). Furthermore, consistent with a recent report (26), LOW-active cells showed a lower relative firing increase during SWRs than did other cells ($p = 4.6 \times 10^{-7}$ and 0.046, Tukey-Kramer test).

Overall, these observations demonstrate that LOW and DOWN states co-occur but are otherwise distinct states.

Oscillatory and spiking activities before and after LOW states

To examine how LOW sleep affects other oscillatory activities seen during non-REM, we detected slow waves (0.5–4 Hz), sleep spindles (10–16 Hz), and sharp wave ripples (SWRs; 140–250 Hz) in the CA1 region LFP, and compared these before, during and after LOW states (Figure 2A). Not surprisingly, the mean amplitudes of hippocampal slow waves (SWA) and the incidences of hippocampal spindles and SWRs were all significantly lower during LOW. To test for more global effects of LOW states, in 8 sessions (from 2 animals), we also detected SWA and spindles on electroencephalogram (EEG) above the neocortical frontal lobe. Interestingly, we observed lower SWA (MI = -0.17 ± 0.004, $p = 4.5 \times 10^{-68}$) and a lower incidence of sleep spindles (MI = -0.67 ± 0.02, $p = 5.4 \times 10^{-63}$) in the neocortical EEG during LOW sleep states. We next investigated the dynamics of activity at the onset and offset of LOW states. The average LFP power spectrum showed diminished oscillatory activity immediately after and before the onsets and offsets to LOW, respectively (Figure1D). Interestingly, both neocortical and hippocampal SWA dropped following transitions to LOW sleep. While hippocampal SWA showed an immediate overshoot after transition out of LOW sleep (Figure 2B), SWA remained diminished in both hippocampus (ΔM = -5.35 ± 0.70%, $p = 2.23 \times 10^{-17}$) and neocortex (ΔM = -14.9 ± 0.98%, p = 3.1 × 10-40), 0.5 – 1.5s after LOW offset, compared to 0.5 – 1.5s before LOW onset. The incidence of spindles and SWRs also dropped and rose sharply at the onsets and offsets of LOW states, respectively. In particular, the SWR incidence peaked 0.1 s before the transitions into and 0.1s after

transitions out of LOW, indicating that SWRs tended to precede as well as follow LOW state transitions. Similar to SWA, these activities did not immediately return to pre-LOW levels (ΔM = -0.177 ± 0.01 s^{-1}, $p = 3.3 \times 10^{-55}$ for SWRs, ΔM = -0.018 ± 0.002 s^{-1}, $p = 1.2 \times 10^{-14}$ for hippocampal spindles, and ΔM = -0.010 ± 0.004 s^{-1}, p = 0.013 for neocortical spindles). Likewise, firing rates of pyramidal cells (ΔM = -0.092 ± 0.004 Hz, $p = 1.7 \times 10^{-92}$), interneurons (ΔM = -0.86 ± 0.06 Hz, $p = 1.2 \times 10^{-30}$) and multi-units (ΔM = -0.059 ± 0.021 Hz, $p = 3.4 \times 10^{-15}$) remained lower for 0.5 – 1.5s after LOW offset, except for in LOW-active cells (Figure 2D). Overall, these oscillatory and spiking activities did not return to pre-LOW levels until ~10s after LOW offset (not shown). In contrast, DOWN states elicited similar modulations but activities did not remain significantly different after the DOWN offset (Figure 2C). Interestingly, both DOWN and LOW states were preceded by transiently increased firing, suggesting a similar onset mechanism, such as a hyperpolarizing current (15, 27). Overall, these analyses demonstrate that oscillatory activities across a wide range of frequencies are strongly diminished during LOW states. Furthermore, these activities transiently increase prior to and immediately following LOW states, but their effect on brain activity lasts beyond the terminus of LOW.

LOW sleep across cortical regions

Based on the modulation of neocortical EEG activities by LOW states, and the neocortical origin of spindles and slow waves detected in the CA1 region (28-30), we hypothesized that LOW states reflect a global decrease of activity throughout the cortex. To test this hypothesis directly, we analyzed additional data from multiple brain regions obtained at http://crcns.org (31, 32). Applying the same detection methods to data from the entorhinal cortex (EC) and the hippocampus of rats recorded by Mizuseki et. al.

(31)(Figure 3A), we confirmed the occurrence of LOW states in hippocampal region CA1. Moreover, we observed coincident LOW states in layer 2/3, and layer 4/5 of the medial entorhinal cortex. LOW states were visually apparent in the spike rasters and LFP of these brain regions. For the dataset recorded by Peyrache et. al. (33) in mice, we found simultaneous LOW states in the medial prefrontal cortex (mPFC), anterodorsal thalamic nucleus (ADn), post-subiculum (PoS) and hippocampus (Figure 3B and C). In both these datasets, the durations and inter-event intervals of LOW states detected in the CA1 region displayed distributions similar to our original dataset (Figure 3D).

Firing rates of neurons were significantly modulated in all brain regions considered: MI = -0.44 ± 0.008 ($p = 5.5 \times 10^{-225}$) in CA1, -0.18 ± 0.040 ($p = 5.6 \times 10^{-6}$) in EC2/3, -0.33 ± 0.09 ($p = 0.0015$) in EC4/5, -0.16 ± 0.010 ($p = 2.1 \times 10^{-31}$) in PoS, -0.13 ± 0.018 ($p = 3.5 \times 10^{-10}$) in mPFC, -0.04 ± 0.007 ($p = 9.5 \times 10^{-11}$) in ADn, Wilcoxon signed-rank test; Figure 3E. The strongest modulation observed in CA1 and weakest (but significant) modulation seen in ADn ($p = 1.8 \times 10^{-196}$, one-way ANOVA). The modulation index was significantly higher in CA1 compared to each of the other brain regions except EC4/5 (Tukey-Kramer test, $p < 10^{-6}$ for each) and significantly lower in ADn than other regions (Tukey-Kramer test, $p < 0.01$ for each). In addition, the cross-correlogram between onsets/offsets of LOW states in CA1 and those in other regions showed clear peak around zero (Figure 3F) with no secondary peaks. Auto-correlograms of LOW onsets/offsets (not shown) also showed no secondary peaks, again indicating that LOW was not reliably cyclic. To assess the temporal propagation of LOW between brain regions, we compared onsets times within 1-s immediately before and after the CA1 LOW onset. Transition rates to LOW were higher in EC2/3, EC4/5, and PoS (ΔM = 0.060 ± 0.015 s^{-1}, $p = 4.5 \times$

10^{-5} for EC2/3, $\Delta M = 0.045 \pm 0.021$ s^{-1}, $p = 0.019$ for EC4/5, $\Delta M = 0.163 \pm 0.014$ s^{-1}, $p = 3.8 \times 10^{-38}$ for PoS) immediately after CA1 LOW onsets, but were greater in mPFC preceding CA1 onset ($\Delta M = -0.060 \pm 0.011$ s^{-1}, $p = 2.2 \times 10^{-9}$) and unchanged in ADn ($\Delta M = 0.002 \pm 0.005$ s^{-1}, $p = 0.650$). These results indicate that LOW states are global and synchronous across brain regions and propagate across cortical regions, with a large fraction initiating earlier in prefrontal regions (34).

Likelihood of LOW decreases within non-REM and increases across sleep

We next examined the occurrence rate of LOW states within non-REM sleep epochs. We observed LOW states throughout both light and dark cycles. In non-REM that followed REM sleep, LOW states were most frequently observed immediately after the end of REM (21), but were present throughout the non-REM epoch (Figure 4A). The percentage of time in LOW was weakly but significantly negatively correlated with the power of theta during the preceding REM epoch ($r = -0.12$, $p = 0.03$). On the other hand, in non-REM epochs that terminated in waking, the likelihood of LOW states increased over time, eventually transitioning into the quiet waking state. Indeed while most (98.3%) LOW states did not terminate in waking, 56.5% of successful transitions from non-REM sleep to waking were transitions out of LOW sleep. Since LOW states were more prevalent following REM sleep and before waking, we conjectured that they may be a signature of a well-rested brain preparing for a potential transition to waking. Based on this conjecture, we predicted that LOW states would be more frequent when sleep pressure is low. Consistent with this conjecture, we found a highly significant negative correlation between SWA (a well-established measure of sleep pressure (35, 36) and evaluated exclusively outside of LOW) and the fraction of time in LOW ($r = -0.30$, $p =$

1.4×10^{-21}; Figure 4B). Moreover, we observed a lower likelihood of LOW states following 3 hrs of prolonged track running (6 – 9 a.m. each day; Figure 4C), when sleep pressure was highest (35, 37), but this likelihood increased and plateaued following sleep.

Additionally, we measured and compared the fraction of time spent in LOW states in extended sleep sequences of REM and non-REM (defined as sleep lasting > 30 min without interruptions > 60 s). Interestingly, the likelihood of LOW states within non-REM increased with time spent sleeping ($r = 0.085$, $p = 0.039$). As an alternate measure, we compared the first and last non-REM epochs within each extended sleep, and found that the fraction of time in LOW increased significantly (change index $CI = 0.21 \pm 0.03$, $p = 3.0 \times 10^{-8}$, Wilcoxon signed-rank test; Figure 4D). Similarly, in non-REM/REM/non-REM triplets, the fraction of time in LOW was higher in the second non-REM (after REM; $CI = 0.11 \pm 0.02$, $p = 2.4 \times 10^{-12}$, Wilcoxon signed-rank test). These changes in the frequency of LOW accounted for a large fraction of the firing rate decreases across sequential non-REM sleep epochs ($R^2 = 0.42$, $p = 2.5 \times 10^{-38}$). However, sleep-dependent firing rates decreased both outside and within LOW states and previously reported correlations (37) between firing decreases and spindles and SWRs remained high when LOW states were excluded ($r = -0.3$ $p < .001$ and $r = -0.22$ $p < .001$ for spindles and SWRs, respectively). In contrast to sleep, after stable waking periods (lasting > 15 min without interruptions > 60 s), the fraction of time in the LOW state decreased following waking but failed to reach significance ($CI = -0.14 \pm 0.08$, $p = 0.071$, Wilcoxon signed-rank test). Finally, following the 3-hr track running sessions the fraction of time in LOW was significantly lower than before the track sessions ($CI = -0.40 \pm 0.13$, $p = 0.031$, Wilcoxon signed-rank test). These results demonstrate that LOW states are more frequent

with increasing sleep, after sleep pressure has dissipated, and less frequent with increased wakefulness, as sleep pressure accumulates.

SIA states in quiet waking

A review of the literature reveals that LOW sleep states share features with SIA and other low activity states observed during quiet waking (12-16, 21, 22). We therefore extended our LOW state detection algorithm to quiet waking periods in our recordings. Durations and inter-event intervals of the detected states during waking, which we refer to as SIA following earlier literature (22, 25, 26, 38), were distributed similarly to sleep LOW, though SIA states were slightly longer (median M = 7.3 s, $p = 5.5 \times 10^{-152}$, Mann–Whitney U test) with shorter inter-event intervals (M = 4.5 s, $p = 5.6 \times 10^{-272}$, Mann–Whitney U test). Interestingly, much of quiet waking qualified as SIA (55.8 ± 1.3 %), compared to 38.3 ± 0.6 % of non-REM in LOW. Unexpectedly, SIA featured more micro-movements than other quiet waking, suggestive of muscle twitches or possibly grooming ($p < 10^{-300}$, Kolmogorov–Smirnov test), but substantially less than active waking ($p < 10^{-300}$, Kolmogorov–Smirnov test).

Next, we compared neuronal activity between LOW states and SIA. Slow waves and spindles were not observed during waking or SIA, but SWRs were. As expected (21), SWR incidence rates were significantly modulated by SIA (MI = -0.40 ± 0.020, $p = 3.8 \times 10^{-51}$, Wilcoxon signed-rank test), and were lower in SIA than in non-REM LOW (Figure 5A). Firing rates of neurons were generally similar in LOW and SIA (Figure 5B). However, some units appeared to be active only during LOW, without firing in SIA (i.e. see 38 points along x-axis of Figure 5B). These cells had no reliable place fields within the home cage (in 37 out of 38 peak place field firing was < 0.3 Hz). Nevertheless,

overall firing rates were slightly higher in SIA than LOW ($p = 1.8 \times 10^{-19}$ for pyramidal cells, 8.0×10^{-7} for multi-unit cluster, and 6.5×10^{-21} for interneurons; Figure 5C).

These differences hint that LOW and SIA are indeed different microstates. We therefore also compared the power spectra of the hippocampal LFP and neocortical EEG between SIA and LOW states (Figure 5D). Overall patterns were similar, but SIA states had significantly lower power < 25.6 Hz in the hippocampal LFP than LOW. These differences were likely due to the absence of slow waves and spindles during awake states. However, we also observed significantly higher power in the gamma band (36.0–87.9 Hz). Similar differences were seen in the neocortical EEG spectrum (Figure 5D). Moreover, hippocampus LFP and neocortical EEG demonstrated enhanced coherence near theta and gamma, suggesting a greater level of consciousness and arousal during SIA. On the other hand, SWA activity in non-REM sleep showed an immediate partial rebound following LOW (Figures 2F & 5E), but not if the animal actually awoke, with high EMG, and was by definition in SIA. Thus, LOW is a microstate *within* non-REM sleep, whereas SIA is an *interruption* of sleep and resets the buildup of SWA (35).

Nevertheless, we wondered whether longer duration LOW states may approach micro-arousals, even if shorter LOWs don't (39). We therefore separated LOW states into long and short LOWs at the median. To avoid potential biases from EMG electrode placement, we measured EMG in two ways, using signals obtained from nuchal electrodes and using volume-conducted signals obtained from intracranial electrodes (40). While long LOW states demonstrated slightly higher EMG, these values were significantly below SIA levels in either of these EMG measures (Figure 5F). Additionally even long LOW epochs featured low power and coherence in gamma (Figure 5G) confirming that sleep LOW

states were not brief wakings, and vice-versa. Most (98.1%) of LOW states transitioned back into non-REM, and very few (1.0 %) directly into quiet waking. On the other hand, it is interesting to note that gamma power was already higher in the small subset (0.9%) of LOW states that transitioned specifically into SIA. Nevertheless, we note that long LOWs were more likely to terminate in waking than short LOWs (Figure 5H), and the fraction of time in SIA decreased between the first and last resting awake epochs during stable waking (Figure 5I), as animals became drowsier and eventually fall asleep. Overall, these observations demonstrate that sleep and SIA states share many features, but are nonetheless distinct.

Discussion (981 words)

In summary, we observed long lasting suppressed activity periods during non-REM sleep, which we call LOW activity sleep. In earlier studies in natural sleep, microstates were observed that share features with the LOW activity sleep states we describe (e.g. 19, 20, 41, 42). However, population spiking activity was not available in those studies and it could not be determined whether these low-amplitude epochs were desynchronized because of high or low neuronal firing activity. Jarosiewicz and colleagues (21, 25) also studied SIA and LOW in large-scale hippocampal unit recordings and made similar observations about neuronal firing and SWRs. Our study provides a quantitative confirmation and extends on their reports.

We showed that LOW sleep was characterized by a strong decrease in population spiking activity, and a parallel decrease in oscillatory activities including slow waves, sleep spindles, and SWRs. While most neuronal activities rebounded after LOW, their levels remained diminished for several seconds, indicating a lingering effect of LOW

states beyond their terminus (39, 43). SWRs, however, were transiently increased immediately before and after LOW, potentially reflecting homeostatic rebound (44), and a possible vulnerability towards epilepsy (45, 46), though we saw no evidence of pathology. We also showed for the first time that LOW states strongly suppress neuronal activity not just in the hippocampus, but throughout the brain, including the entorhinal cortex, prefrontal cortex, post subiculum and anterodorsal thalamus. This suppressed activity lasted much longer than is typical for DOWN states and was marked by increased firing in a subset of LOW-active neurons. We showed the LOW sleep occurred not just after REM but throughout non-REM sleep, and is likely triggered in response to high neuronal activity, from either REM sleep or UP states and SWRs (7, 37). Importantly, we uncovered an inverse relationship between the rate (fraction of time) of LOW sleep and sleep pressure, with low likelihood in early non-REM sleep following waking, but increasing likelihood following sleep and the release of sleep pressure. Finally, we were able to demonstrate that LOW states are distinctly a sleep state, with lower EMG, lower gamma and gamma coherence, and greater SWA rebound than SIA or quiet waking.

Some confusion may unfortunately arise from inconsistent terminology in the literature. For example, LOW sleep states were called “S-SIA” by Jarosiewicz et. al. (21), but later “SIA” by the same authors (25, 38) and more recently, by Kay et. al. (26). They also appear to share features with phase B of the cyclic alternating pattern (CAP) in non-REM sleep (39, 42, 47). Furthermore, a recent study witnessed events similar to SIA, with high waking-level EMG, but referred to these as microarousals (43). We propose that SIA should be reserved for the waking state, as originally described by Vanderwolf (22) and later employed by others (21), while LOW amplitude/LOW activity sleep is best

reserved for the sleep state, as also originally used (19, 20). Nevertheless, it is possible that collectively LOW sleep and waking SIA represent the sleep and waking extremes of a continuum of microarousals (43, 48), with LOW states potentially transitioning into SIA under appropriate (Figures 5F-H). Consistent with this idea, SIA states (relative to LOW) showed higher gamma power and gamma coherence between hippocampal LFP and neocortical EEG, consistent with consciousness, and hippocampal place-cells that encode the animal's sleep location begin to fire during both LOW sleep and SIA (21, 25, 26), as if in preparation for spatial cognition (49).

Vyazovskiy and Harris (11) recently proposed that a global quiescent state may be valuable for cellular repair and restoration of organelles. They suggested the DOWN state during non-REM may play such a role. Since LOW states provide a longer decrease in global activity than DOWN states, LOW states may in fact be more suitable for carrying out such functions. The neuronal activities that occur in non-REM outside of LOW states (e.g. slow waves, spindles, and SWRs) have been linked to some of the memory benefits of sleep (1, 2, 50). We found that within extended sleep sequences of non-REM and REM cycles, LOW states were more dominant in late sleep, whereas slow waves, spindles and SWRs are more prevalent in early sleep (37). These observation, combined with the greater fidelity of replay during early sleep (51, 52), may support the idea that early sleep serves for circuit modification, including synaptic downscaling (1, 10), while late sleep, under decreased sleep pressure, may provide for cellular restoration and upkeep (11, 53). Nevertheless, further research is necessary to better understand the role of LOW states in carrying out the functions of sleep.

LOW and SIA also appear to share features with the low-activity phase of infra-slow oscillations (12-16), though we observed no evidence for repeated oscillatory cycles in LOW (Figure 1E). Recent evidence suggests the low-activity phases of infra-slow oscillations are produced by long-lasting hyperpolarizing potassium currents, mediated by ATP-derived adenosine released from astrocytes (15). Such non-synaptic currents may produce LOW states, potentially accounting for the parallel firing decreases observed in both pyramidal cells and interneurons. Furthermore, we note that there was also a lingering effect from LOW states on subsequent activity patterns (see also ref(43)). Interestingly, infra-slow low-activity phases coincide with large-scale calcium waves in astrocytic networks (54), which may account for their global nature. Cerebral blood flow during these low-activity phases is ~10% lower, indicating that they are detectable in global BOLD activity as well as LFP (17). Given these facts, along with the central role that astrocytes and adenosine play in cellular repair (55), energy metabolism (56), and mediating sleep pressure (57), we believe that they play a central role in the genesis and function of LOW states. It is also interesting to note that LOW states are most prevalent immediately following REM sleep, during which neuronal firing rates are relatively high (7, 37). Such high firing may increase the brain's need for rest and restoration that is subsequently provided by LOW activity sleep.

Materials and Methods

We analyzed data from hippocampal region CA1 with neocortical EEG described in a previous study (37), along with data from CA1 and entorhinal cortex (58), and from anterodorsal thalamus, and post-subiculum and medial prefrontal cortex (33), freely available at http://crcns.org (31, 32). Details of methods, including surgery, unit clustering, local field spectrum analysis, sleep state, slow-wave, spindle, and sharp-wave ripple detections, are provided elsewhere (37).

Animals, surgery, and data collection. Four male Long-Evans rats (250-350g; Charles River Laboratories, Wilmington, MA) were anesthetized with isoflurane and implanted with silicon microprobes in the dorsal hippocampus (2.00 mm lateral and 3.36 mm posterior from the bregma). In three of the rats, 2 stainless steel wires (AS 636, Cooner wire, Chatsworth, CA) were placed into the nuchal muscles to measure the electromyograph (EMG). Electrical coherence in microprobe electrodes in the 300-600 Hz band was also used as an alternate measure of EMG (40, 43). We took filtered signals from the top channel of each shank and calculated mean pair-wise correlations among electrode pairs separated $\geq$ 400 µm in 0.5-s bins. These two measures were independent but strongly correlated ($r = 0.63$ in 5-s time bins). In two of the rats, screws were inserted on the skull above the right frontal lobe (3.00 mm lateral and 2.50 mm anterior from the bregma) and attached to Nyleze insulated copper wires (overall diameter 0.13 mm; Alpha Wire, Elizabeth, NJ). The signals were recorded with a Digital Lynx recording system (Neuralynx, Bozeman, MT), then processed using previously described methods (59) After a recovery period from surgery (> 5 days), rats were placed on a water-restriction regimen to motivate track running, and were given ad-libitum water for 30 mins each

day. Three out of four rats were maintained in a home cage except during the last 3 h of dark cycles, during which they were put on an I-, L-, or U-shaped linear track in the same room and given water rewards on platforms after every traversal. A fourth rat was recorded only in the home cage during the light cycle. Two colored light-emitting diodes were mounted on the headstage and the animals' movements were tracked with an overhead video camera. All procedures were in accordance with the National Institutes of Health guidelines and approved by the University of Wisconsin-Milwaukee Institutional Animal Care and Use Committee.

Unit clustering and cell classification. Unit clustering and cell classification were performed as previously described (59). We analyzed light cycles and dark cycles separately. For track-running sessions, we concatenated data from behavior on the track with the last 3 hrs of the preceding dark cycle (pre-sleep) and the first 3 hrs of the following light cycle (post-sleep). Putative pyramidal cells and interneurons were separated based on standard methods using spike waveforms, burstiness, refractory periods, and firing rates (60-62). Units with an isolation distance < 15 (63) were considered potentially multi-units.

Spectral analyses. LFP, EMG and EEG traces were low-pass filtered at 1250 or 1280 Hz using NDManager and its plugins (64)(http://ndmanager.sourceforge.net). Power spectra were whitened and calculated using multitaper methods and the Chronux toolbox for Matlab (65) in 1-s windows.

Sleep and behavioral state detection. Sleep and waking were separated based on nuchal EMG and the animal's movement. Sleep was detected by low nuchal EMG power and no movement (defined below). The remainder was considered waking. EMG signals were

first smoothed with a 1-s Gaussian filter and power was z-scored in 500-ms overlapping windows at 100-ms steps. A two-threshold "Schmitt" trigger was used to detect transitions between "low" and "high" EMG power at 0 and 0.5 threshold z scores. Similarly, the thresholds for "no movement" and "movement" were set at 0.5 cm/s and 5 cm/s. Transient (< 10 s) low or high EMG power or movement states were ignored. Detected states underwent post-hoc visual inspection and occasional manual modification. In one rat for which nuchal EMG was not recorded, no movement followed by slow waves signaled non-REM sleep. REM was inferred from high theta (described below) with no movement sandwiched between non-REM epochs. Transitions from non-REM to resting awake were identified at time points when the mean hippocampal slow wave amplitude (defined below in 5-s bins) dropped < 80% of the maximum reached in the non-REM epoch. Data from this animal was consistent with the rest, but was excluded from EMG analyses (Figure 5F and G). The theta (5-10 Hz) over (1-4 Hz plus 10-14 Hz) band ratio of the power spectral density was used to detect transitions between high theta and low theta, using custom-made MATLAB software written by Anton Sirota (61) based on the Hidden Markov Model Toolbox for Matlab (Kevin Murphy), followed by visual inspection. Sleep states with high theta were classified as REM (rapid eye movement) and the remainder were classified as non-REM (66, 67). Similarly, waking periods with high theta were labeled "active awake" and the remainder were labeled "resting awake." For the Peyrache et al. (32) dataset, we used the provided non-REM, REM, and wakefulness timestamps, and considered only epochs > 50 sec.

Sharp-wave ripple detection. SWRs were detected following previously described methods (68). First, the ripple band (130-230Hz) power of the LFP was calculated during

non-REM and quiet waking. Channels with the largest power in the ripple band were selected for each shank, and periods with power exceeding 1 SD of the mean at least one of the selected channels were labeled as candidate events. Candidates with short gaps (< 50ms) were combined. Candidates shorter than 30 ms or longer than 450 ms were abandoned. Candidates were classified as SWRs if their peak power was greater than 5 SDs of the mean.

Sleep spindle detection. Hippocampal LFP and neocortical EEG were band-pass filtered between 10–16 Hz (nearly identical results were observed with a wider 9–18 Hz band (37)). For hippocampal spindles, the channel with the largest mean power during non-REM sleep was used. Candidate spindles in each signal were detected when amplitudes of the Hilbert transform exceeded 1.5 SDs above the mean for longer than 350 ms (69). Candidates were concatenated when inter-event intervals were shorter than 125 ms. Candidates with peak amplitudes below 4 SDs above the mean were abandoned. For each candidate, spindle troughs were detected. Candidates with inter-trough intervals longer than 125 ms (corresponding to slower than 8 Hz) were discarded.

Slow wave detection. We used a previously established method (7, 37, 70) to detect individual slow waves in the neocortical EEG and the hippocampal LFP as positive deflections between two negative deflections in the band-pass filtered signal (0.5 - 4 Hz). The polarity of the hippocampal LFP was inverted due to the polarity reversal relative to the EEG (71). Slow waves separated by less than 100-ms were discarded. Slow wave activity (SWA) was defined by the amplitude of these individual slow waves measured from trough to peak.

LOW activity sleep detection. LOW states were detected based on the power spectra of the LFP in each brain region calculated in 1-s windows sliding with 0.1-s steps. The average power between 0 – 50 Hz was Gaussian filtered (σ = 0.5 s) and z-scored based on mean and SD within non-REM sleep. Histogram of filtered power during non-REM had two peaks (Figure 1B). We determined the position of lower peak and the local minimum between the two peaks based on second derivative of smoothed (Gaussian filter, σ = 0.1 z-score) histogram. Periods in which z-scored power was lower than the local minimum were detected as candidate LOW states. If the LFP power in a candidate LOW did not drop below the lower peak of the histogram, it was discarded. Two consecutive LOW states separated by < 0.5 s were concatenated. We used the same thresholds to detect SIA in resting awake.

For analyses in Figure 2, which required more accurate timestamps, onsets and offsets were determined from population (MUA) firing rates. First, the mean firing rate in previously detected LOW and bordering non-LOW intervals were calculated. The threshold for each LOW onset/offset was set to the mean firing rate in LOW plus 20% of the difference with bordering non-LOWs and onset and offset timestamps were shifted accordingly.

DOWN/DOWN' state detection. Hippocampal DOWN states arise from neocortical influence during SWA (28-30). DOWN states during non-REM were defined as periods with no CA1 units spiking for ≥ 50 ms (7, 23, 67, 72). To test whether LOW states might be equivalent to long-lasting DOWN states under relaxed assumptions, we detected low-firing periods (DOWN' states) by thresholding Gaussian filtered (σ = 100 ms) multi-unit activity (MUA) in 50-ms bins within non-REM sleep (24). The threshold for each session

was set at the value for which the median MUA was equivalent within DOWN' and LOW states.

Modulation/Change indices. LOW modulation index (MI) for variable X was defined as $(X_{LOW} - X_{non\text{-}LOW}) / (X_{LOW} + X_{non\text{-}LOW})$. The change index (CI) for X was defined by $(X_{post} - X_{pre})/(X_{post} + X_{pre})$.

LOW/DOWN' modulated cells. Spikes were counted in 100-ms bins, then means within LOW and DOWN' states were calculated. The same number of bins were then randomly selected from outside of LOW, to calculate surrogate means. This procedure was iterated 2000 times within each session separately. If the mean within LOW/DOWN' was higher (or lower) than top (or bottom) 0.5% of the shuffled data, the cell marked as activated (or suppressed). We obtained qualitatively similar results with a novel community detection method (73).

Figure Legends

Figure 1

LOW activity microstates during non-REM sleep. (A) Two representative recordings from hippocampal region CA1 from different animals. Top panels show raster plots of mean firing rates in 1-s bins (179 [/108] pyramidal cells, 13 [/2] interneurons and 42 [/3] multi-unit clusters for Rat 1 [/Rat 2], ordered by mean firing rates). Colors indicate firing rates normalized to the session mean. EMG traces are shown above. Colors in band beneath the raster indicate detected brain states (pink, purple, dark blue, and light blue correspond to resting awake, LOW states within non-REM, non-LOW states in non-REM, and REM, respectively). Bottom panels show power spectrograms of hippocampal LFP. White lines indicate raw LFP traces. (B) Histograms of z-scored LFP power < 50 Hz in different brain states. The non-REM histogram has two peaks, reflecting LOW and non-LOW states. (C) Zoomed examples (corresponding green boxes) from panel A. (D) LOW state onset- and offset-triggered CA1 LFP power spectra (n = 14,369, for LOW > 2 s) showed diminished power upon transition into LOW states, with partial resumption after the offset. (E) Firing rates of neurons were lower within LOW states during non-REM. Orange, blue and green indicate pyramidal cells (n = 1599), interneurons (n = 138) and multi-unit clusters (n = 213), respectively. Black line is the identity. Right panel shows modulation indices (S.E.M. error bars) of pyramidal cells, interneurons and multi-unit clusters. (F) Durations and inter-event intervals of LOW states and DOWN' states (see Methods and Materials) differed. Top panel shows distribution of LOW durations (n = 15,573). Vertical line indicates median = 5.2 s. Bottom panel shows distribution of inter-event intervals of LOW (n = 14,402). Vertical line indicates median = 10.5 s. For

comparison, duration and inter-event intervals of DOWN' states are superimposed with cyan (median of duration [/inter event intervals] = 450 [/400] ms, n = 298,806 [/297,853] events). (G) Firing rates within LOW and DOWN' states were similar, by definition (colors as in panel E). (H) Most cells decreased firing within LOW states (1,445 pyramidal cells, 106 interneurons, and 195 multi-unit clusters), but a small number of "LOW-active" cells (see Materials and Methods) increased firing (95 pyramidal cells, 31 interneurons, and 2 multi-unit clusters). Some cells' firing did not change significantly (59 pyramidal cells, 1 interneurons, and 16 multi-unit clusters). In contrast, very few cells apparently increased firing within DOWN' (14 pyramidal cells, 1 interneuron, and 0 multi-unit clusters), and only 4 pyramidal cells (0 interneurons or multi-units) had unchanged firing during DOWN' states. ** $p < 0.01$, *** $p < 0.001$.

Figure 2

LOW states modulated by network oscillations during non-REM. (A) Left three panels show slow-wave amplitudes (SWA) in hippocampus (HPC; green) and neocortex (NC; gray), the incidence rates of HPC spindles (magenta), NC spindles (cyan) and HPC SWRs (yellow) in different non-REM epochs (n = 931 for HPC and n = 416 for NC). Right panel shows modulation indices (S.E.M. error bars) for these oscillatory events. (B, C) Peri-event triggered histograms of oscillatory events and neuronal firings. (B) SWA (top) decreased after transitions to LOW states (n = 14,369 LOW states > 2 s), and partially rebounded after transitions out of LOW states in both HPC (green; peak at 0.2 s) and NC (gray). Incidences of spindles and SWRs (middle) decreased upon LOW onset. NC spindle changes (left axis, cyan) were delayed (~ 0.5 s) relative to the HPC. LOW states were often preceded by SWRs (right axis, yellow; peak at 0.1 s) and followed by

rebound SWRs (peak at 0.1s). Mean firing rates (bottom) of pyramidal cells (*n*= 1599 cells, orange, left axis), interneurons (*n* = 138 cells, blue, right axis) and multi-unit activity (*n* = 213 cells, green, left axis) transiently increased before the onset and following the offset of LOW states, likely because of SWRs. (C) Modulation of SWA (top) and spindles and SWRs incidence rates (middle), and neuronal firing (bottom) by DOWN states (*n* = 1,255,479). Note the shorter timescales compared to panel C. (D) LOW-active pyramidal cells (*n* = 95) showed increased firing during LOW, following a transient decrease. In contrast, the same cells showed decreased firing in DOWN' states > 2s, despite some overlap between DOWN' and LOW. The same patterns were seen in LOW-active inhibitory cells and multi-units (not shown). Error bars indicate S.E.M, *** p <0.001.

Figure 3

LOW states across different brain regions. (A-C) Examples of LOW states in datasets obtained in rat by Mizuseki et al. (31) (A) and in mice by Peyrache and Buzsaki (32) (B & C) and Top panels show spike raster plots in 1-s bins. Color indicates brain regions, and brightness indicates firing rates normalized to the session means (50 CA1 cells, 5 EC2/3 cells, and 17 EC4/5 cells in A; 6 CA1 multi-units, 18 mPFC cells and 46 ADn cells in B; 20 PoS cells and 10 ADn cells in C). Middle panels depict power spectra of simultaneously recorded LFPs. Bottom panels show detected LOW states separately for these regions, illustrating frequent synchrony across regions. (D) Durations and inter-event intervals were distributed similarly across data sets and brain regions. Left panels show the histograms of durations and inter-event intervals for CA1 LOW states in data sets recorded by us (black, *n* = 14238 [/14094] for duration [/inter-event interval]),

Mizuseki et al. (31) (dark gray, n = 794 [/772] for duration [/inter-event interval]), and Peyrache and Buzsaki (32) (light gray, n = 11606 [/11418] for duration [/inter-event interval]). Vertical lines indicate median values. Right panels show the histograms of durations and inter-event intervals in LOW states detected in EC2/3 (dark yellow n = 2131 [/2082] for duration [/inter-event interval]), EC4/5 (light yellow n = 977 [/946] for duration [/inter-event interval]), PoS (magenta, n = 10590 [/10459] for duration [/inter-event interval]), mPFC (green, n = 1833 [/1788] for duration [/inter-event interval]) and ADn (cyan n = 19558 [/19336] for duration [/inter-event interval]). Vertical lines indicate median values. (E) Neuron firing rates were modulated by LOW states in all brain regions (n = numbers of cells, indicated above; S.E.M. error bars). (F) Cross-correlograms between LOW states in CA1 and other brain regions show that LOW states onsets (top) and offsets (bottom) occurred largely synchronously. ** $p < 0.01$, *** $p < 0.001$.

Figure 4

LOW states increased with decreasing sleep pressure over sleep. (A) The fraction of time in LOW decreased within non-REM epochs followed by REM (blue, n = 423 non-REM epochs, $p = 3.5 \times 10^{-16}$, one-way ANOVA followed by Tukey-Kramer tests), but increased within non-REM epochs followed by resting awake (red, n = 233 non-REM epochs, $p = 1.3 \times 10^{-4}$, one-way ANOVA followed by Tukey-Kramer tests). The fraction of time in DOWN states was unchanged within non-REM epochs followed by either REM (light green) or awake (dark green). (B) SWA, calculated exclusively outside of LOW, was inversely correlated with the fraction of time in LOW states (n = 953 non-REM epochs). Regression line (cyan) is superimposed on density map of epoch means.

(C) The fraction of time in LOW states was lowest immediately following 3-hr track running sessions (from 6 – 9 a.m. each day), gradually increasing and stabilizing. Background colors indicates % of time spent in each behavioral/sleep state. (D) The fraction of time in LOW increased across sleep and decreased after wakefulness. Change indices between non-REM epochs interleaved by REM (n = 308) and between the first and last non-REM epochs in extended sleep (n = 109) were significantly > 0. In contrast, those between non-REM epochs immediately before and after 3-hr track sessions (n = 7) were significantly < 0, while those between the first and last non-REM epochs in stable waking episodes (n = 38) decreased without reaching significance. * p <0.05, ** p < 0.01, *** p < 0.001, error bars indicate S.E.M.

Figure 5

Comparison of LOW and SIA states. (A) Incidence rates of SWRs were lower in SIA than in LOW sleep. (B) Mean firing rates of pyramidal cells (orange, n = 1599), interneurons (blue, n = 138) and multi-units (green, n = 213) were similar in LOW and SIA. However, 25 pyramidal cells and 13 multi-unit clusters fired during LOW but not SIA (see x-axis; black line shows the identity). (C) Mean firing rates of pyramidal cells and interneurons were higher in SIA than in LOW. (D) Power spectra of hippocampal LFP and neocortical EEG (left 2 panels), and coherence between these regions (right 2 panels) show significant differences in theta and gamma frequency bands (significance bands indicated in gray, p < 0.01 and black, p < 0.001, Mann–Whitney U test with Bonferroni correction). (E) Mean SWA is compared between transitions from quiet waking to non-REM (solid lines, n = 570 [/265] events for the hippocampus [/neocortex]) and transitions from LOW to non-REM (dashed lines, see Figure 2C). (F) EMG

amplitudes obtained from nuchal muscles (top) and derived from intracranial electrodes (bottom). Left traces are aligned to the transition from non-REM to LOW and from resting awake to SIA. Right traces are aligned from LOW to SIA, from LOW to non-REM, and from SIA to resting awake (right). LOW transitions to SIA were marked by increasing EMG amplitudes (n = 229 events). EMG remained high during transitions from resting awake to SIA (n = 3189). EMG showed small increases during long (LOW > 5.6s, n = 5779), but not short LOW (n = 6194). (G) Mean gamma (45 – 65 Hz) power of the HPC LFP (top) and NC EEG (middle) decreased upon transition from resting awake to SIA (n = 3730 [/1435] for HPC [/NC]) and upon transitions from non-REM to long (n = 6674 [/2359]) and short LOW (n = 6775 [/3255]). Increases were observed in the reverse transitions (n = 3741 [/1447] SIA to resting awake, n = 6798 [/2376] long LOW to non-REM, and n = 6813 [/3277] short LOW to non-REM, for HPC [/NC]). Gamma power also increased at the transition from SIA to LOW (n = 254 [/132]). Gamma band coherence differences did not reach significance using this analysis, but showed non-significant decreases from non-REM to LOW (n = 2359 [/3255] for long [/short] LOW) and recovered at transition from LOW to non-REM (n = 2376 [/3277] for long [/short] LOW). No changes were observed from resting awake to SIA (n = 1435) or SIA to resting awake (n = 1447). LOW to SIA transitions are omitted due to high variability, but were consistent with resting awake/SIA transitions. (H) Transitions to awake occurred more frequently following long compared to short LOWs ($p = 7.4\times10^{-5}$, chi-squared test). Dashed line indicate mean across all LOW states. (I) SIA states became less likely with increased waking (n = 162 resting awake epochs over 47 stable waking (>15 min) periods). The likelihood of LOW states decreased between the first and last

resting awake epochs in stable wakings. Significance was tested against 5000 random shuffles. ** $p < 0.01$, *** $p < 0.001$, error bars indicate S.E.M. and shading indicates 95% confident intervals.

References

1. Tononi G & Cirelli C (2014) Sleep and the price of plasticity: from synaptic and cellular homeostasis to memory consolidation and integration. *Neuron* 81(1):12-34.
2. Rasch B & Born J (2013) About sleep's role in memory. *Physiol Rev* 93(2):681-766.
3. Buzsaki G (1989) Two-stage model of memory trace formation: a role for "noisy" brain states. *Neuroscience* 31(3):551-570.
4. Rechtschaffen A (1998) Current perspectives on the function of sleep. *Perspect Biol Med* 41(3):359-390.
5. Steriade M, Nunez A, & Amzica F (1993) A novel slow (< 1 Hz) oscillation of neocortical neurons in vivo: depolarizing and hyperpolarizing components. *J Neurosci* 13(8):3252-3265.
6. Buzsaki G (2015) Hippocampal sharp wave-ripple: A cognitive biomarker for episodic memory and planning. *Hippocampus* 25(10):1073-1188.
7. Vyazovskiy VV, *et al.* (2009) Cortical firing and sleep homeostasis. *Neuron* 63(6):865-878.
8. Sirota A & Buzsaki G (2005) Interaction between neocortical and hippocampal networks via slow oscillations. *Thalamus Relat Syst* 3(4):245-259.
9. Born J & Wilhelm I (2012) System consolidation of memory during sleep. *Psychol Res* 76(2):192-203.

10. Tononi G & Cirelli C (2003) Sleep and synaptic homeostasis: a hypothesis. *Brain Res Bull* 62(2):143-150.

11. Vyazovskiy VV & Harris KD (2013) Sleep and the single neuron: the role of global slow oscillations in individual cell rest. *Nat Rev Neurosci* 14(6):443-451.

12. Chan AW, Mohajerani MH, LeDue JM, Wang YT, & Murphy TH (2015) Mesoscale infraslow spontaneous membrane potential fluctuations recapitulate high-frequency activity cortical motifs. *Nat Commun* 6:7738.

13. Aladjalova NA (1957) Infra-slow rhythmic oscillations of the steady potential of the cerebral cortex. *Nature* 179(4567):957-959.

14. Hiltunen T, *et al.* (2014) Infra-slow EEG fluctuations are correlated with resting-state network dynamics in fMRI. *J Neurosci* 34(2):356-362.

15. Lorincz ML, Geall F, Bao Y, Crunelli V, & Hughes SW (2009) ATP-dependent infra-slow (<0.1 Hz) oscillations in thalamic networks. *PloS One* 4(2):e4447.

16. Filippov IV, Williams WC, Krebs AA, & Pugachev KS (2008) Dynamics of infraslow potentials in the primary auditory cortex: component analysis and contribution of specific thalamic-cortical and non-specific brainstem-cortical influences. *Brain Res* 1219:66-77.

17. He B & Raichle M (2009) The fMRI signal, slow cortical potential and consciousness. *Trends Cogn Sci* 13(7):302-309.

18. Logothetis NK & Wandell BA (2004) Interpreting the BOLD signal. *Annual review of physiology* 66:735-769.

19. Pickenhain L & Klingberg F (1967) Hippocampal slow wave activity as a correlate of basic behavioral mechanisms in the rat. *Prog Brain Res* 27:218-227.

20. Bergmann BM, Winter JB, Rosenberg RS, & Rechtschaffen A (1987) NREM sleep with low-voltage EEG in the rat. *Sleep* 10(1):1-11.

21. Jarosiewicz B, McNaughton BL, & Skaggs WE (2002) Hippocampal population activity during the small-amplitude irregular activity state in the rat. *J Neurosci* 22(4):1373-1384.

22. Vanderwolf CH (1971) Limbic-diencephalic mechanisms of voluntary movement. *Psychol Rev* 78(2):83-113.

23. Johnson LA, Euston DR, Tatsuno M, & McNaughton BL (2010) Stored-trace reactivation in rat prefrontal cortex is correlated with down-to-up state fluctuation density. *J Neurosci* 30(7):2650-2661.

24. Ji D & Wilson MA (2007) Coordinated memory replay in the visual cortex and hippocampus during sleep. *Nat Neurosci* 10(1):100-107.

25. Jarosiewicz B & Skaggs WE (2004) Hippocampal place cells are not controlled by visual input during the small irregular activity state in the rat. *J Neurosci* 24(21):5070-5077.

26. Kay K, *et al.* (2016) A hippocampal network for spatial coding during immobility and sleep. *Nature* 531(7593):185-190.

27. Compte A, Sanchez-Vives MV, McCormick DA, & Wang XJ (2003) Cellular and network mechanisms of slow oscillatory activity (<1 Hz) and wave propagations in a cortical network model. *J Neurophysiol* 89(5):2707-2725.

28. Isomura Y, *et al.* (2006) Integration and segregation of activity in entorhinal-hippocampal subregions by neocortical slow oscillations. *Neuron* 52(5):871-882.

29. Hahn TT, Sakmann B, & Mehta MR (2006) Phase-locking of hippocampal interneurons' membrane potential to neocortical up-down states. *Nat Neurosci* 9(11):1359-1361.

30. Hahn TT, McFarland JM, Berberich S, Sakmann B, & Mehta MR (2012) Spontaneous persistent activity in entorhinal cortex modulates cortico-hippocampal interaction in vivo. *Nat Neurosci* 15(11):1531-1538.

31. Mizuseki K, *et al.* (2014) Neurosharing: large-scale data sets (spike, LFP) recorded from the hippocampal-entorhinal system in behaving rats. *F1000Res* 3:98.

32. Peyrache A & Buzsáki G (2015) Extracellular recordings from multi-site silicon probes in the anterior thalamus and subicular formation of freely moving mice. . *CRCNSorg*.

33. Peyrache A, Lacroix MM, Petersen PC, & Buzsaki G (2015) Internally organized mechanisms of the head direction sense. *Nat Neurosci* 18(4):569-575.

34. Massimini M, Huber R, Ferrarelli F, Hill S, & Tononi G (2004) The sleep slow oscillation as a traveling wave. *J Neurosci* 24(31):6862-6870.

35. Achermann P, Dijk DJ, Brunner DP, & Borbely AA (1993) A model of human sleep homeostasis based on EEG slow-wave activity: quantitative comparison of data and simulations. *Brain Res Bull* 31(1-2):97-113.

36. Borbely AA & Achermann P (1999) Sleep homeostasis and models of sleep regulation. *J Biol Rhythms* 14(6):557-568.

37. Miyawaki H & Diba K (2016) Regulation of Hippocampal Firing by Network Oscillations during Sleep. *Curr Biol* 26(7):893-902.

38. Jarosiewicz B & Skaggs WE (2004) Level of arousal during the small irregular activity state in the rat hippocampal EEG. *J Neurophysiol* 91(6):2649-2657.

39. Halasz P, Terzano M, Parrino L, & Bodizs R (2004) The nature of arousal in sleep. *J Sleep Res* 13(1):1-23.

40. Schomburg EW, *et al.* (2014) Theta phase segregation of input-specific gamma patterns in entorhinal-hippocampal networks. *Neuron* 84(2):470-485.

41. Roldan E, Weiss T, & Fifkova E (1963) Excitability Changes during the Sleep Cycle of the Rat. *Electroencephalogr Clin Neurophysiol* 15:775-785.

42. Terzano MG, *et al.* (1985) The cyclic alternating pattern as a physiologic component of normal NREM sleep. *Sleep* 8(2):137-145.

43. Watson BO, Levenstein D, Greene JP, Gelinas JN, & Buzsaki G (2016) Network Homeostasis and State Dynamics of Neocortical Sleep. *Neuron* 90(4):839-852.

44. Girardeau G, Cei A, & Zugaro M (2014) Learning-induced plasticity regulates hippocampal sharp wave-ripple drive. *J Neurosci* 34(15):5176-5183.

45. Penttonen M, *et al.* (1999) Ultra-slow oscillation (0.025 Hz) triggers hippocampal afterdischarges in Wistar rats. *Neuroscience* 94(3):735-743.

46. Vanhatalo S, *et al.* (2004) Infraslow oscillations modulate excitability and interictal epileptic activity in the human cortex during sleep. *Proc Natl Acad Sci* 101(14):5053-5057.

47. Parrino L, Ferri R, Bruni O, & Terzano MG (2012) Cyclic alternating pattern (CAP): the marker of sleep instability. *Sleep Med Rev* 16(1):27-45.

48. Halasz P (1998) Hierarchy of micro-arousals and the microstructure of sleep. *Neurophysiol Clin* 28(6):461-475.

49. O'Keefe JM & Nadel L (1978) *The hippocampus as a cognitive map* (Clarendon Press; Oxford University Press, Oxford, New York) pp xiv, 570 p.

50. Buzsaki G (1998) Memory consolidation during sleep: a neurophysiological perspective. *J Sleep Res* 7 Suppl 1:17-23.

51. Kudrimoti HS, Barnes CA, & McNaughton BL (1999) Reactivation of hippocampal cell assemblies: effects of behavioral state, experience, and EEG dynamics. *J Neurosci* 19(10):4090-4101.

52. Tatsuno M, Lipa P, & McNaughton BL (2006) Methodological considerations on the use of template matching to study long-lasting memory trace replay. *J Neurosci* 26(42):10727-10742.

53. Genzel L, Kroes MC, Dresler M, & Battaglia FP (2014) Light sleep versus slow wave sleep in memory consolidation: a question of global versus local processes? *Trends Neurosci* 37(1):10-19.

54. Kuga N, Sasaki T, Takahara Y, Matsuki N, & Ikegaya Y (2011) Large-scale calcium waves traveling through astrocytic networks in vivo. *J Neurosci* 31(7):2607-2614.

55. Chen Y & Swanson RA (2003) Astrocytes and brain injury. *J Cereb Blood Flow Metab* 23(2):137-149.

56. Porkka-Heiskanen T & Kalinchuk AV (2011) Adenosine, energy metabolism and sleep homeostasis. *Sleep Med Rev* 15(2):123-135.

57. Halassa MM, *et al.* (2009) Astrocytic modulation of sleep homeostasis and cognitive consequences of sleep loss. *Neuron* 61(2):213-219.

58. Mizuseki K, Sirota A, Pastalkova E, & Buzsaki G (2009) Theta oscillations provide temporal windows for local circuit computation in the entorhinal-hippocampal loop. *Neuron* 64(2):267-280.

59. Diba K & Buzsaki G (2008) Hippocampal network dynamics constrain the time lag between pyramidal cells across modified environments. *J Neurosci* 28(50):13448-13456.

60. Csicsvari J, Hirase H, Czurko A, & Buzsaki G (1998) Reliability and state dependence of pyramidal cell-interneuron synapses in the hippocampus: an ensemble approach in the behaving rat. *Neuron* 21(1):179-189.

61. Sirota A, *et al.* (2008) Entrainment of neocortical neurons and gamma oscillations by the hippocampal theta rhythm. *Neuron* 60(4):683-697.

62. Bartho P, *et al.* (2004) Characterization of neocortical principal cells and interneurons by network interactions and extracellular features. *J Neurophysiol* 92(1):600-608.

63. Schmitzer-Torbert N, Jackson J, Henze D, Harris K, & Redish AD (2005) Quantitative measures of cluster quality for use in extracellular recordings. *Neuroscience* 131(1):1-11.

64. Hazan L, Zugaro M, & Buzsaki G (2006) Klusters, NeuroScope, NDManager: a free software suite for neurophysiological data processing and visualization. *J Neurosci Methods* 155(2):207-216.

65. Bokil H, Andrews P, Kulkarni JE, Mehta S, & Mitra PP (2010) Chronux: a platform for analyzing neural signals. *J Neurosci Methods* 192(1):146-151.

66. Robinson TE, Kramis RC, & Vanderwolf CH (1977) Two types of cerebral activation during active sleep: relations to behavior. *Brain Res* 124(3):544-549.

67. Grosmark AD, Mizuseki K, Pastalkova E, Diba K, & Buzsaki G (2012) REM sleep reorganizes hippocampal excitability. *Neuron* 75(6):1001-1007.

68. Diba K, Amarasingham A, Mizuseki K, & Buzsáki G (2014) Millisecond timescale synchrony among hippocampal neurons. *J Neurosci* 34(45):14984 – 14994.

69. Sullivan D, Mizuseki K, Sorgi A, & Buzsaki G (2014) Comparison of sleep spindles and theta oscillations in the hippocampus. *J Neurosci* 34(2):662-674.

70. Vyazovskiy VV, Cirelli C, & Tononi G (2011) Electrophysiological correlates of sleep homeostasis in freely behaving rats. *Prog Brain Res* 193:17-38.

71. Nir Y, *et al.* (2011) Regional slow waves and spindles in human sleep. *Neuron* 70(1):153-169.

72. Luczak A, Bartho P, Marguet SL, Buzsaki G, & Harris KD (2007) Sequential structure of neocortical spontaneous activity in vivo. *Proc Natl Acad Sci U S A* 104(1):347-352.

73. Billeh YN, Schaub MT, Anastassiou CA, Barahona M, & Koch C (2014) Revealing cell assemblies at multiple levels of granularity. *J Neurosci Methods* 236:92-106.

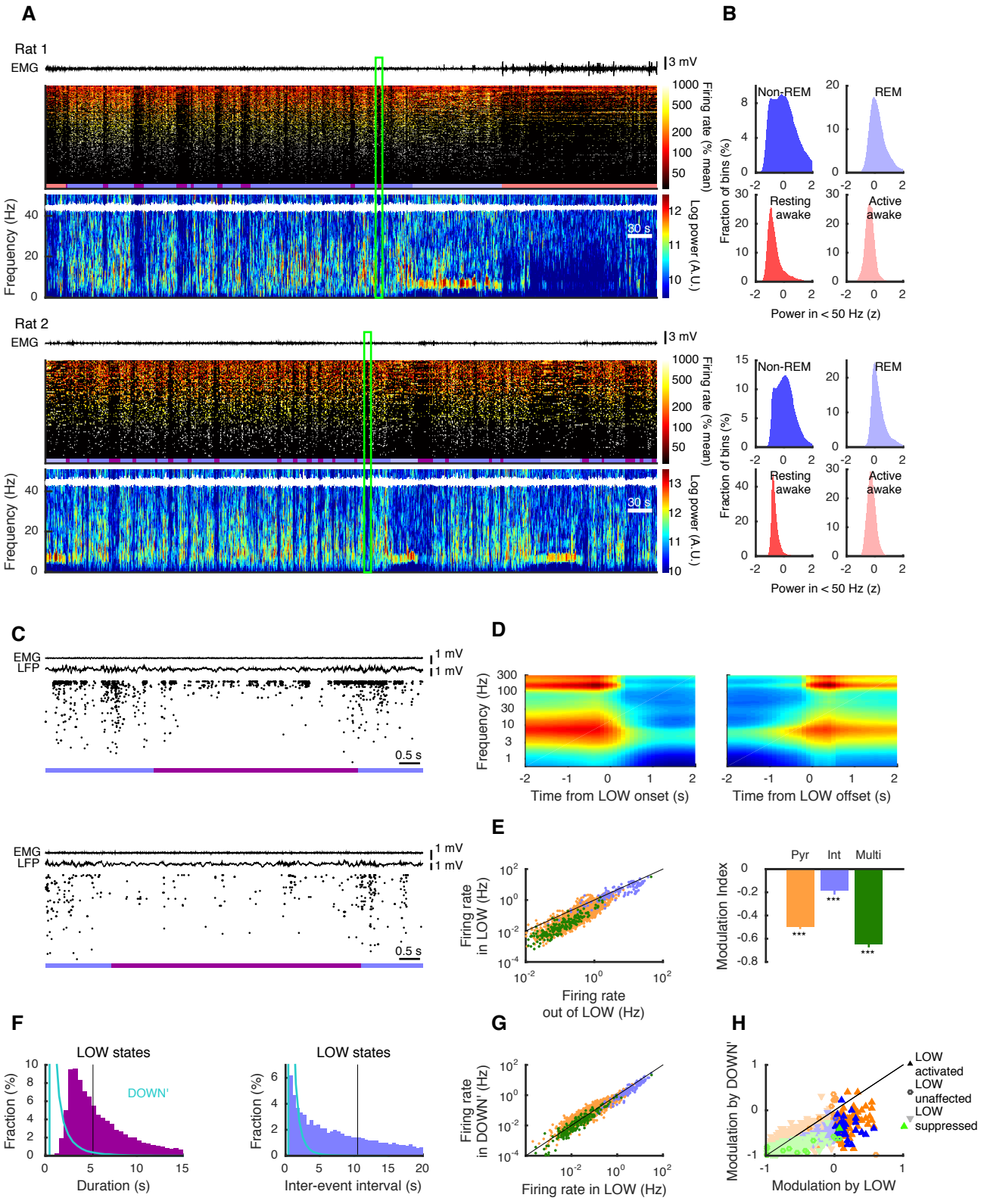

Figure 1

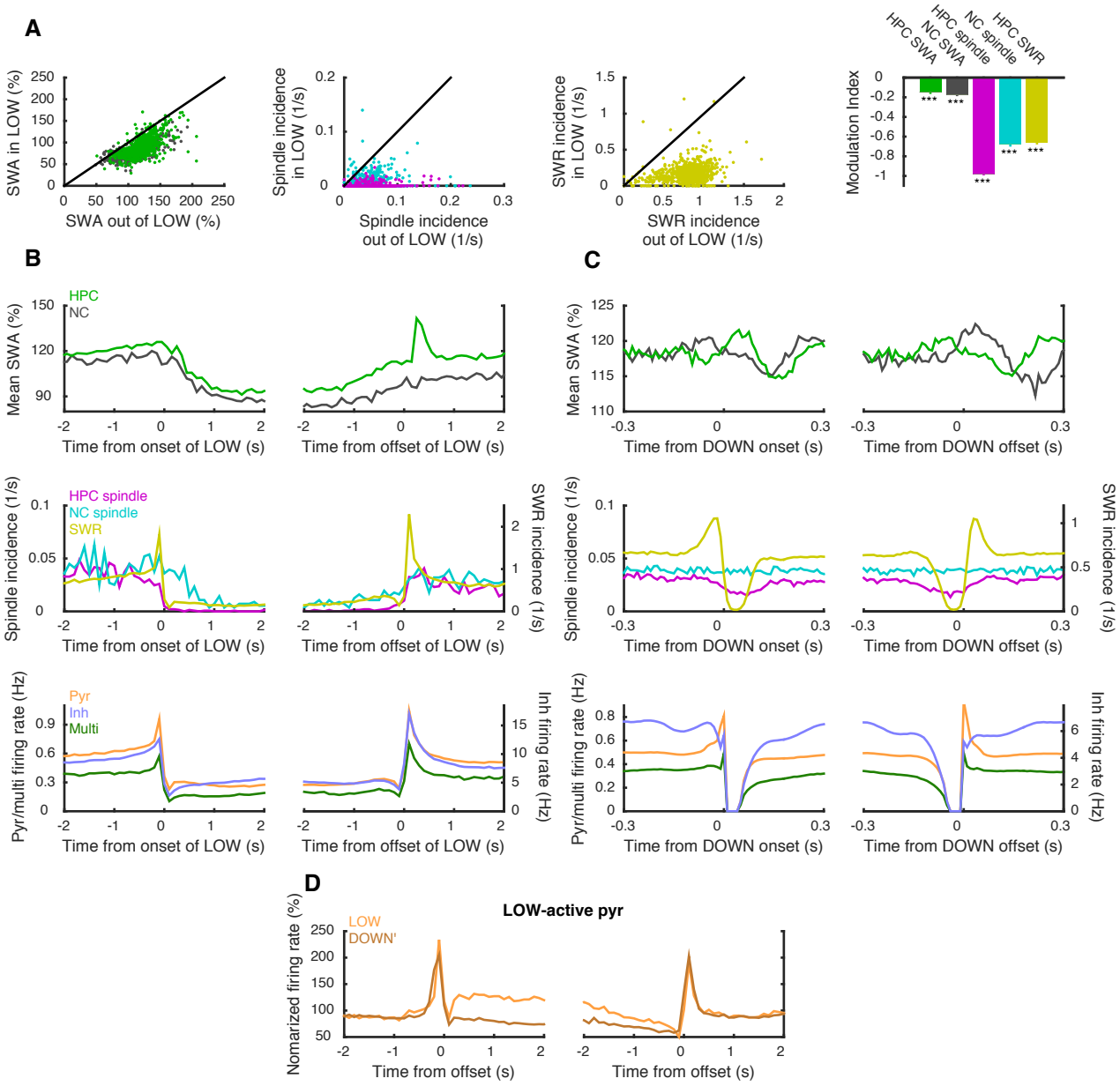

Figure 2

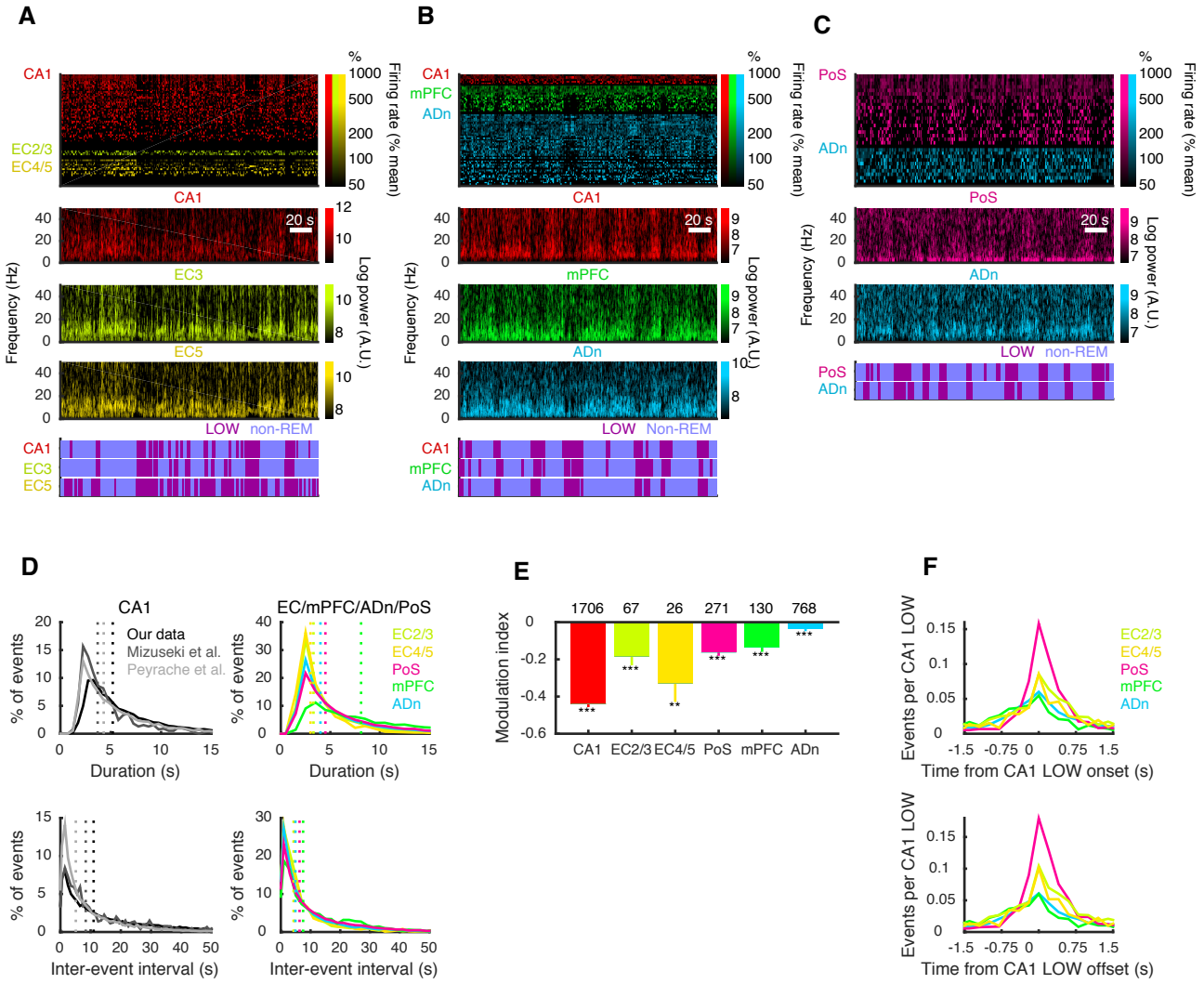

Figure 3

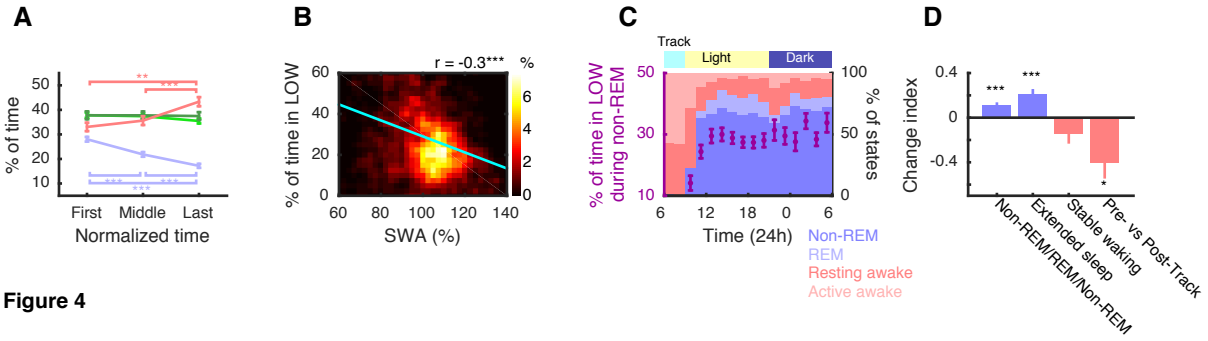

Figure 4

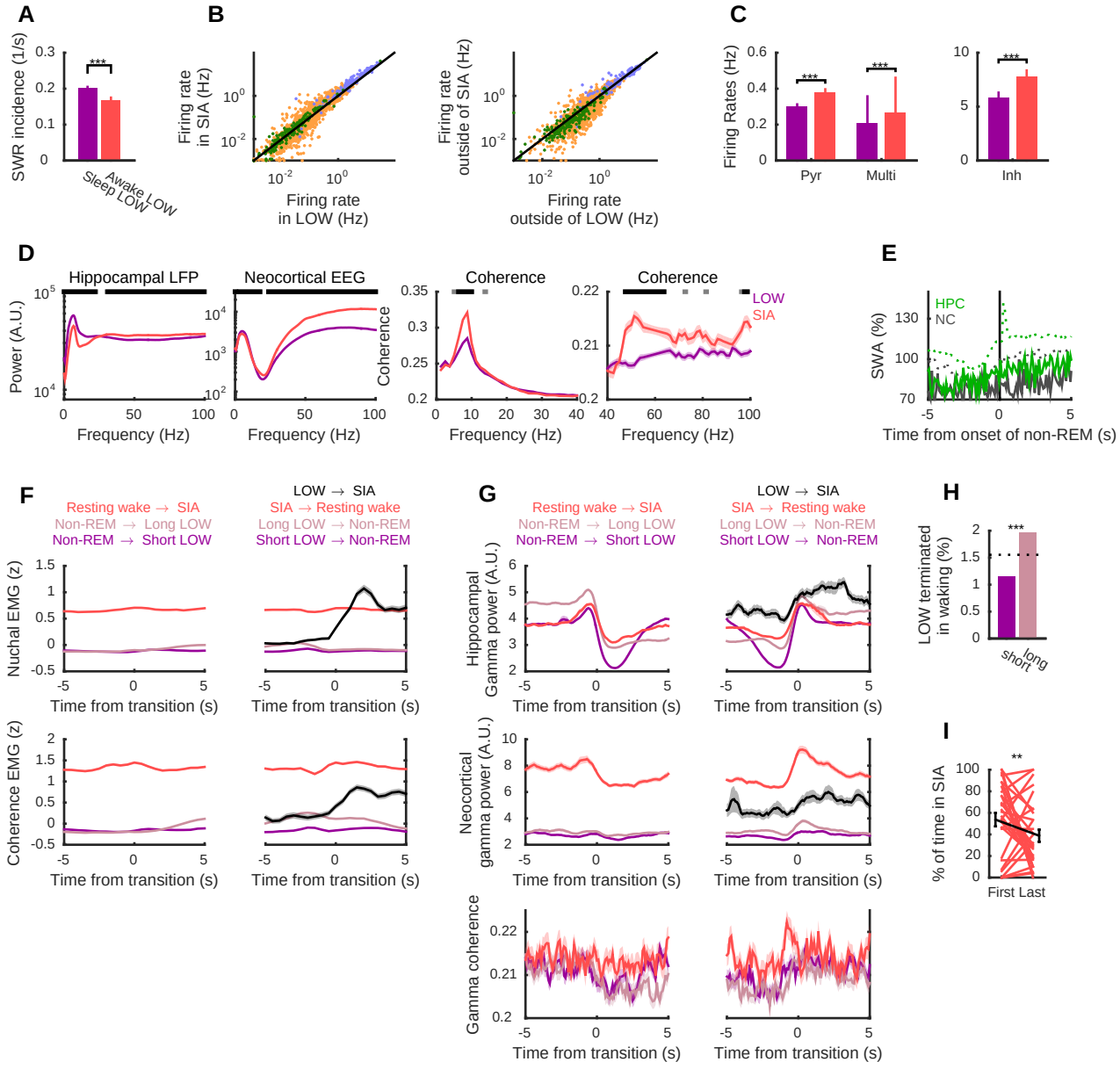

Figure 5